Supplementary Information (SI) for Chemical Science.
This journal is © The Royal Society of Chemistry 2025

A Leigh Syndrome mutation perturbs long-range energy coupling in respiratory complex I

Franziska Hoeser[a], Patricia Saura[b], Caroline Harter[a], Ville R. I. Kaila[b] and Thorsten Friedrich[a]

[a] Institut für Biochemie, Albert-Ludwigs-Universität Freiburg, Germany.

[b] Department of Biochemistry and Biophysics, Stockholm University, Sweden.

Correspondence to ville.kaila@dbb.su.se
Friedrich@bio.chemie.uni-freiburg.de

Supplementary Information

This file includes:

Supplementary Figures S1 to S8
Supplementary Tables S1 to S4
Supplementary References

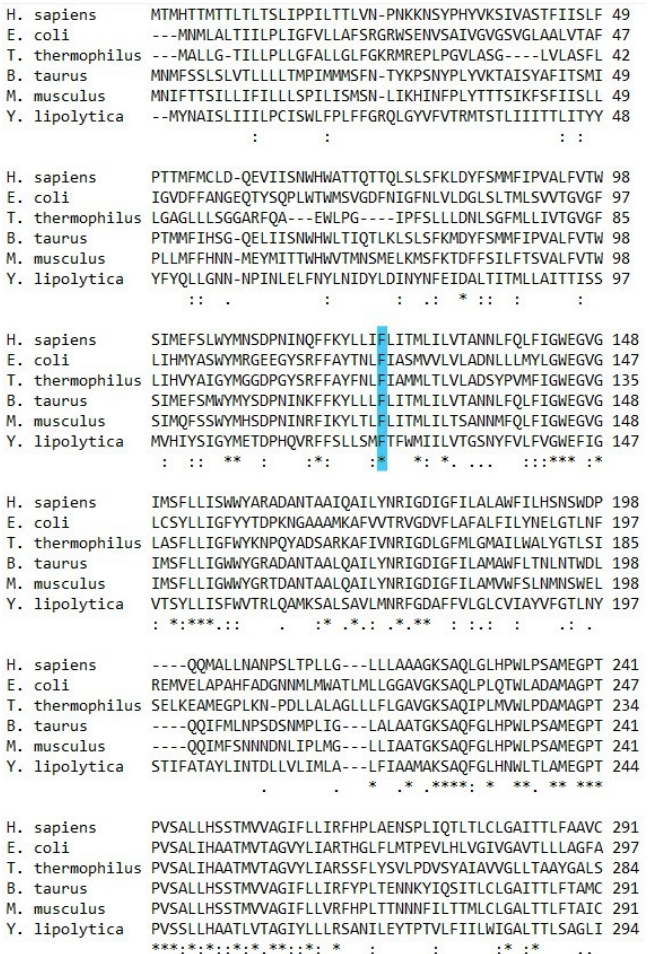

Figure S1. Multiple sequence alignments of ND5 (human = NuoL in *E. coli*). The sequences from *Homo sapiens*, *E. coli*, *T. thermophilus*, *Bos taurus*, *Mus musculus* and *Y. lipolytica* are shown exemplarily. 58 sequences were used to generate the alignments. The position of residue F124 (human numbering) is highlighted in blue. The homologous position in *E. coli* is F123. Residues marked with a star are conserved through the aligned organisms; the colon marks similar and the point slightly similar positions.

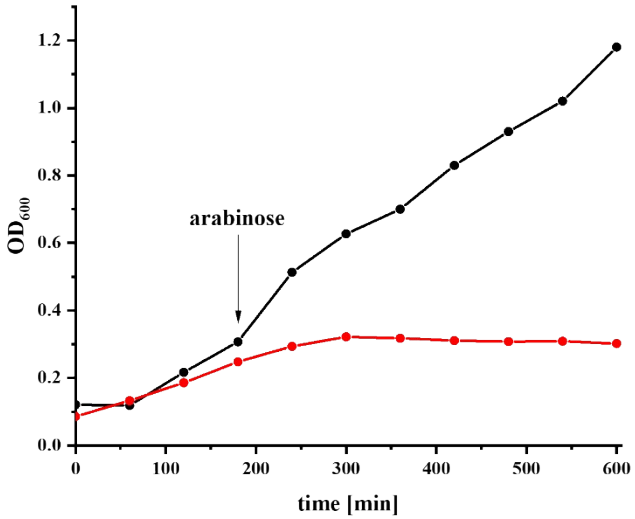

Figure S2. Growth curves of *E. coli* wild type (black) and mutant strain (red) in minimal medium with acetate as sole carbon source. The black arrow indicates induction of gene expression after 3 h by an addition of 0.02% arabinose.

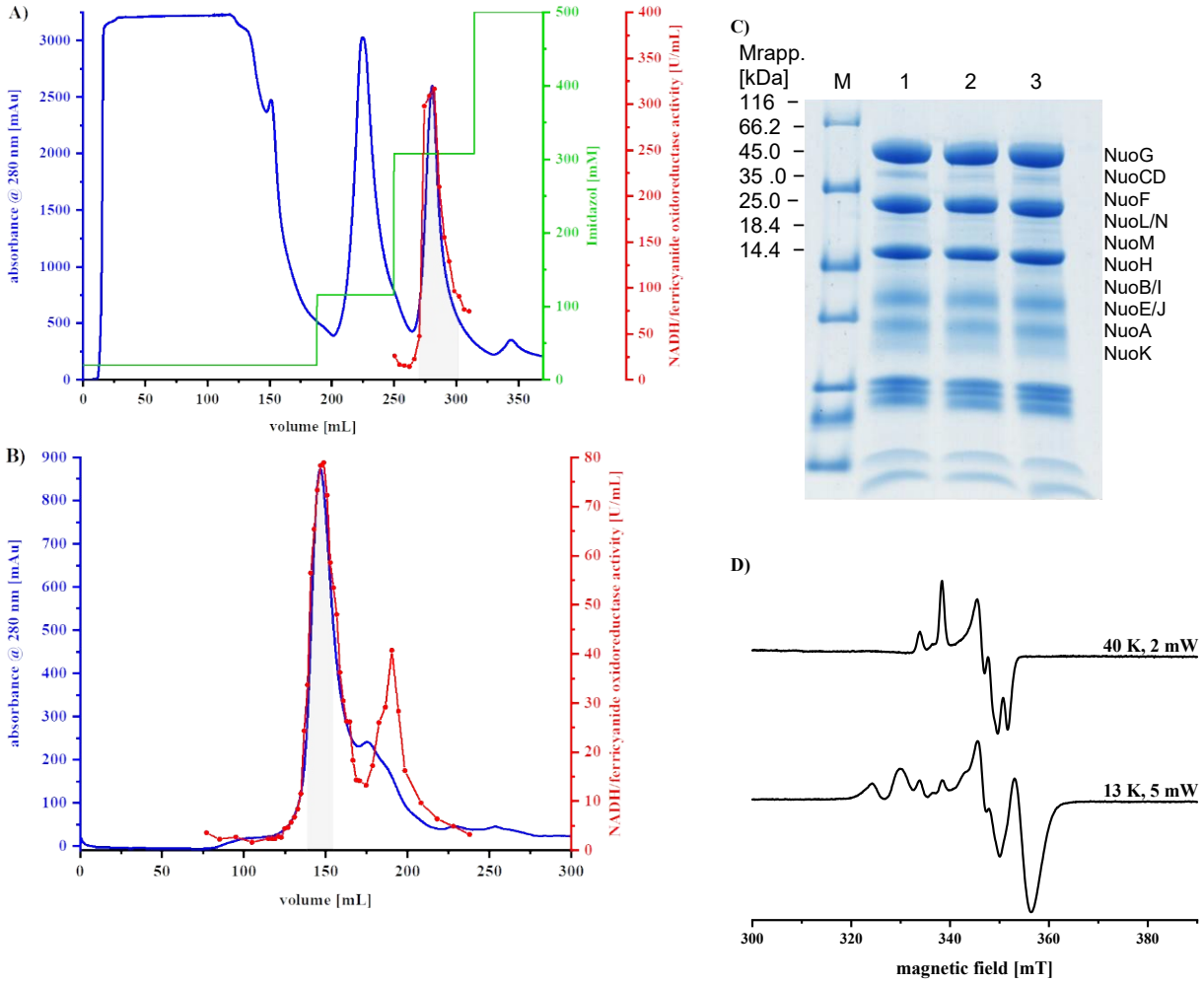

Figure S3. Isolation of complex I and the F123L^{L} variant by A) affinity-chromatography on ProBond Ni^{2+}-IDA and B) size exclusion chromatography on Superose 6. Main fractions of activity indicated with a slightly gray background were used in the next step. Preparations of the wild type and the variant showed virtually identical elution profiles. **C)** SDS-PAGE showing the band patterns of the marker (M) and of the preparations of complex I (1), the D199G^{H} variant (2; described in[23]) and of the F123L^{L} variant (3; this paper). The preparations contain all subunits of complex I. The faint band at around 80 kDa is a proteolytic digestion product of NuoG.[85] **D)** EPR spectra of the preparation of the F123L^{L} variant reduced with NADH at 40 K and 2 mW (top) and at 13 K and 5 mW (bottom).

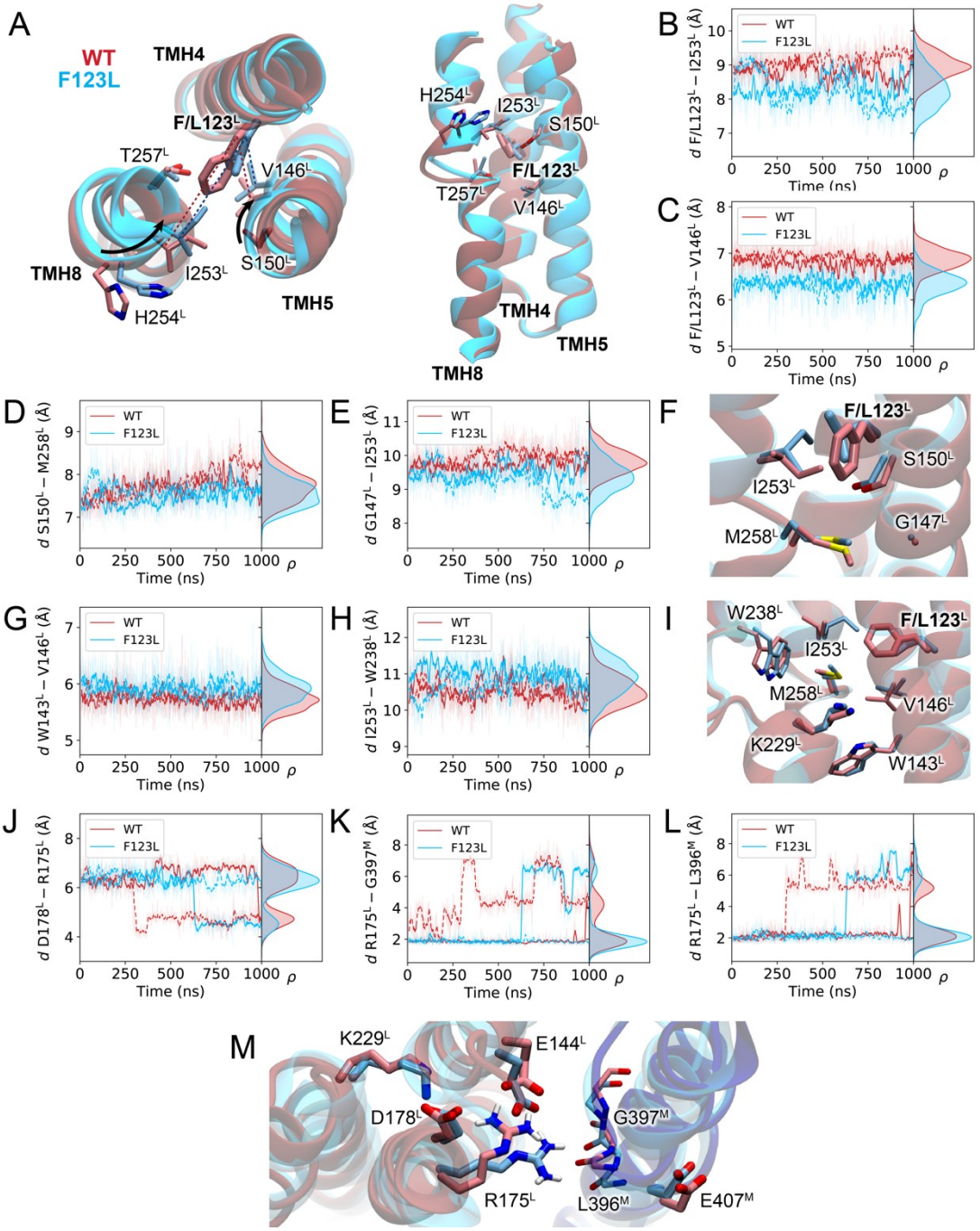

Figure S4. Dynamics of key residues in complex I and the F123L^{L} variant from MD simulations. Red traces correspond to MD simulations of complex I, and light-blue traces to those of the F123L^{L} variant. **A**) Overview of the region around the mutation, showing residues in contact with the affected position. Red structure corresponds to complex I, and light-blue to the variant. Left: top view; right: front view. The mutation decreases the TMH4-THM5 and THM4-THM8 contacts around position 123. **B**) F/L123^{L}(C_{β})-I253^{L}(C_{β}) distance; **C**) F/L123^{L}(C_{β})-V146^{L}(C_{β}) distance; **D**) S150^{L}(C_{β})-M258^{L}(C_{β}) distance; **E**) G147^{L}(C_{α})-I253^{L}(C_{β}); **F**) Close-up of the region around residues displayed in **D**) and **E**); **G**) W143^{L}(C_{β})-V146^{L}(C_{β}) distance; **H**) W238^{L}(C_{β})-I253^{L}(C_{β}) distance; **I**) Close-up of the region around residues displayed in **G**) and **H**); **J**) D178^{L}(C_{γ})-R175^{L}(C_{ζ}) distance; **K**) R175^{L}(H_{η})-G397^{M}(O (C=O)) distance; **L**) R175^{L}(H_{η})-L396^{M}(O (C=O)) distance; **M**) The NuoL/NuoM interface region, showing residues displayed in **J-L**) and their surroundings.

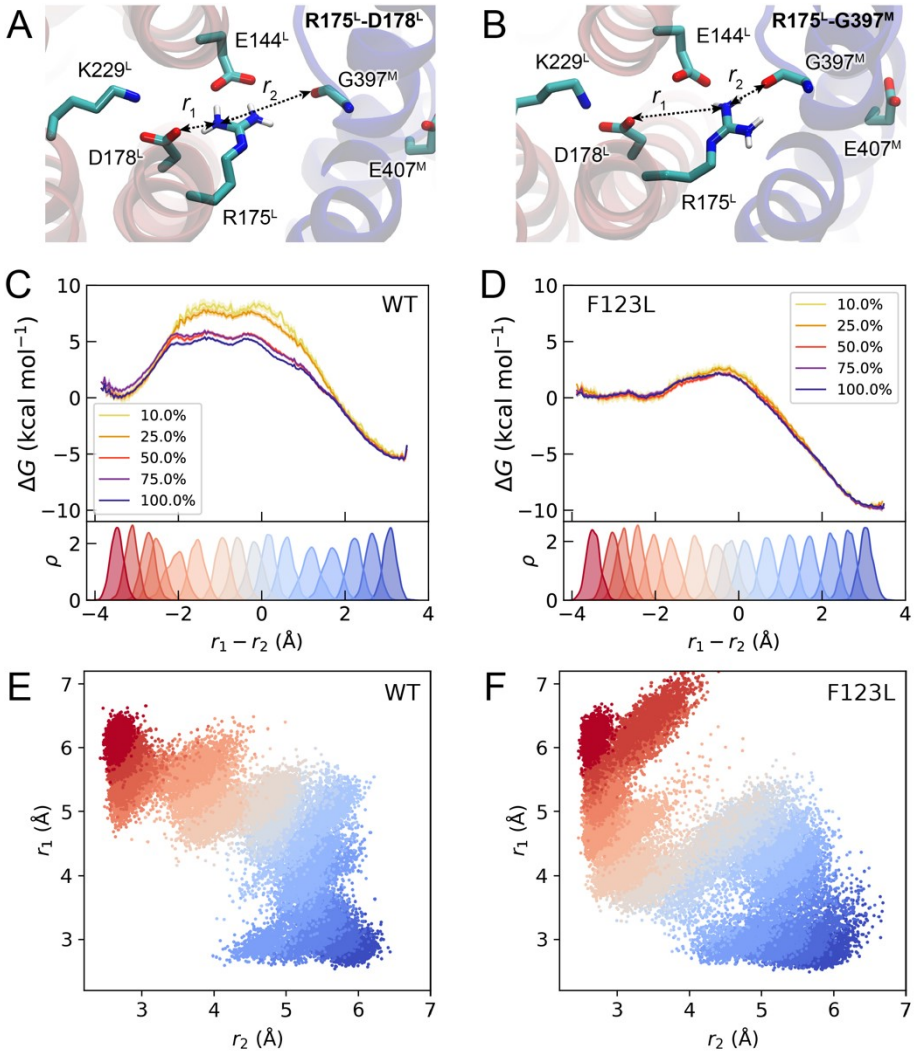

Figure S5. Analysis of free energy calculations. A-B) Representation of the reaction coordinate, defined as distance difference between R175^{L}-D178^{L} (r_1= R175^{L}($N_{\eta 2}$)-D178^{L}($O_{\delta 1}$), and R175^{L}-G397^{M} (r_2 = R175^{L}($N_{\eta 2}$)-G397^{M}(O (backbone C=O oxygen); reaction coordinate = $r_1 - r_2$). **A**) Structure with a R175^{L}-D178^{L} contact ($r_1 < r_2$); **B**) structure with a R175^{L}-G397^{M} contact ($r_1 > r_2$). **C-D**) Convergence of the free energy profiles of (**C**) complex I and (**D**) the F123L variant, as a function of the total sampling (320 ns for the full reaction coordinate; 20 ns/window), showing the overlap of the windows at the bottom. **E-F**) Overlap of the sampled distances (r_1 vs. r_2), for the individual windows (colored as in panels **C-D**), for (**E**) complex I and (**F**) the F123L variant.

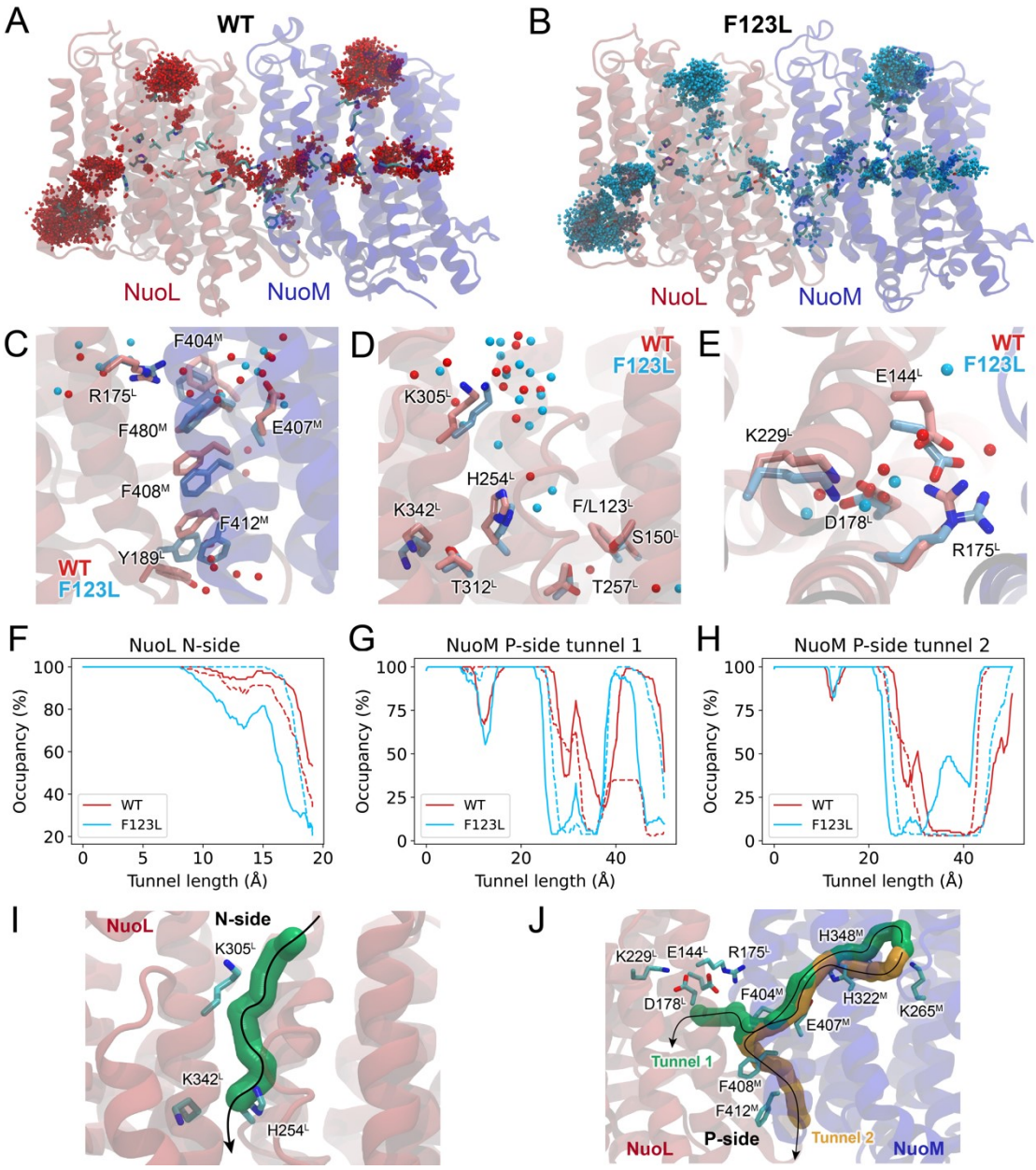

Figure S6. Hydration dynamics in complex I and the F123L^{L} variant. A-B) Hydration around subunits NuoL and NuoM in complex I (**A**) and the F123L^{L} variant (**B**), averaged over 1 μs trajectory. **C-E**) MD snapshots of complex I (water molecules/side chains in red) and F123L^{L} variant (water molecules/side chains in light-blue), showing **C**) P-side region at the NuoL/M interface; **D**) N-side region in NuoL and **E**) ion-pair in NuoL. **F**) Hydration percentage around the N-side proton entry pathway in NuoL (shown in panel (**I**)), averaged over the last 100 ns of the MD trajectory. **G-H**) Hydration percentage around the P-side exit pathway at the NuoM/L interface averaged over the last 100 ns of the simulations, with the tunnels represented in **J** (tunnel 1 (**G**) in green, tunnel 2 (**H**) in orange).

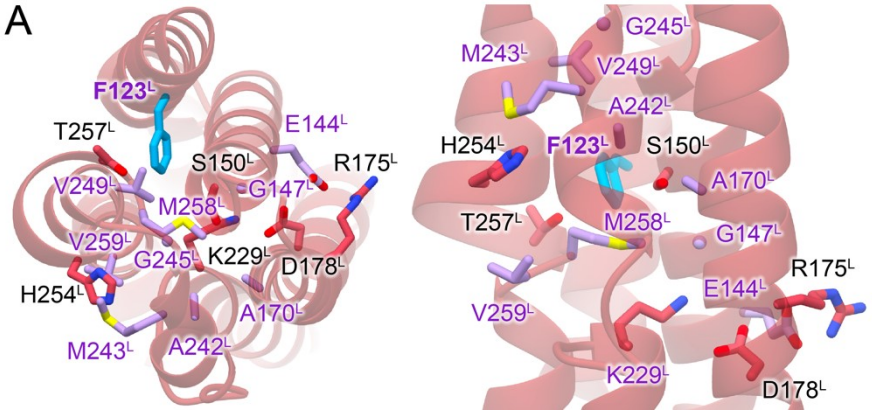

B

Human	*E. coli*
E145^{ND5}	E144^{L}
G148^{ND5}	G147^{L}
A171^{ND5}	A170^{L}
A236^{ND5}	A242^{L}
M237^{ND5}	M243^{L}
G239^{ND5}	G245^{L}
V243^{ND5}	V249^{L}
M252^{ND5}	M258^{L}
V253^{ND5}	V259^{L}

Figure S7. Residues involved in disease-related mutations near F123^{L}. A) Top view (left) and side view (right) of the region near F123^{L} (shown in cyan), showing residues found in disease-related mutants (in purple), and other relevant conserved residues (in red) in the region. **B**) Residue numbering in human and *E. coli* complex I.[23,56-58,60]

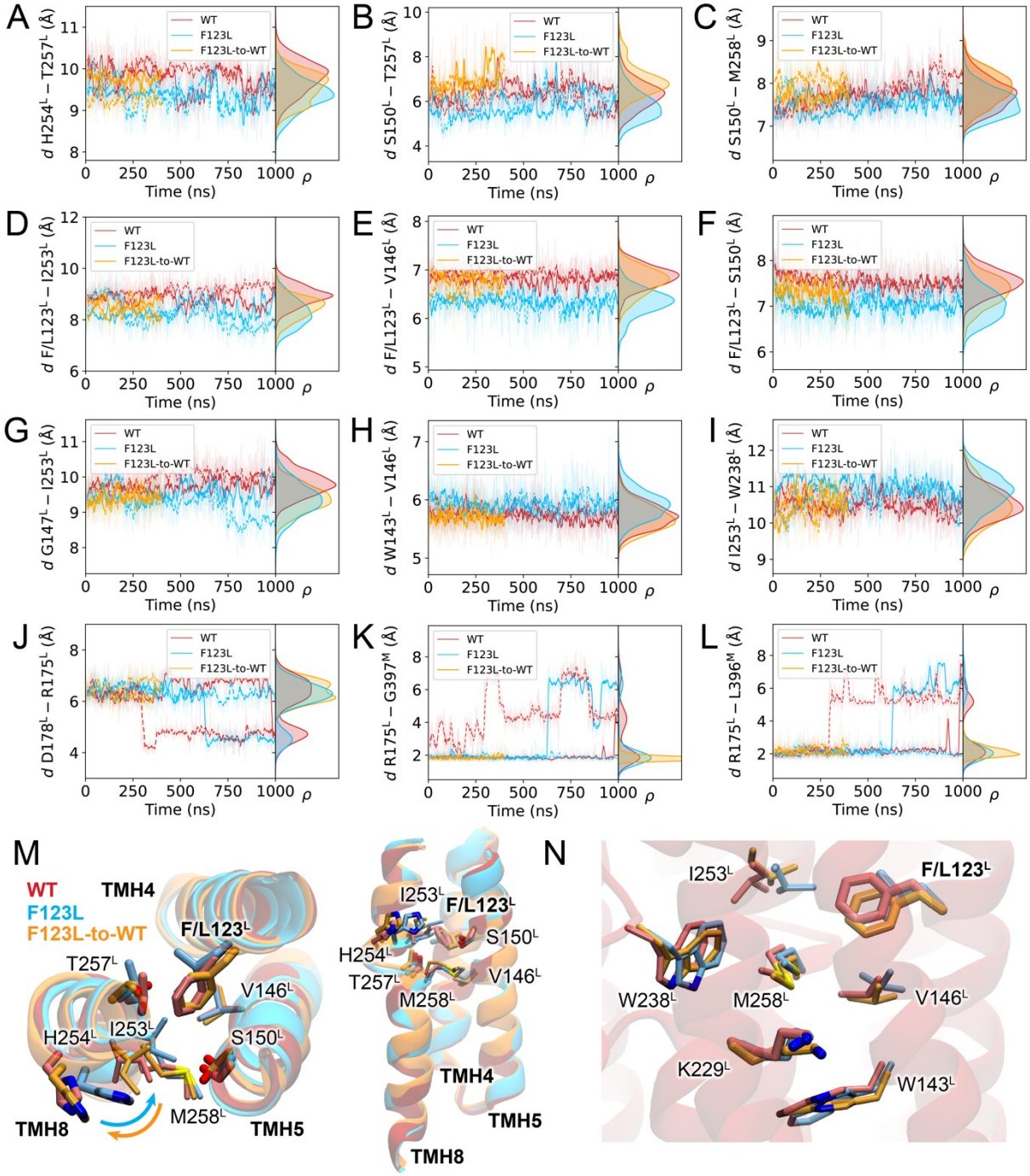

Figure S8. Effect of reverting the F123L^{L} back to complex I in the dynamics of key residues. Orange traces correspond to MD simulations of the F123L reverted back to complex I (F123-2-WT), red traces correspond to the original complex I, and light-blue traces to the F123L^{L} variant. **A**) H254^{L}(C_{γ}) -T257^{L}(C_{β}) distance; **B**) S150^{L}(O_{γ})-T257^{L}(O_{γ}) distance; **C**) S150^{L}(C_{β})-M258^{L}(C_{β}) distance; **D**) F/L123^{L}(C_{β})-I253^{L}(C_{β}) distance; **E**) F/L123^{L}(C_{β})-V146^{L}(C_{β}) distance; **F**) F/L123^{L}(C_{β})-S150^{L}(C_{β}) distance; **G**) G147^{L}(C_{α})-I254^{L}(C_{β}); **H**) W143^{L}(C_{β})-V146^{L}(C_{β}) distance; **I**) W238^{L}(C_{β})-I253^{L}(C_{β}) distance; **J**) D178^{L}(C_{γ})-R175^{L}(C_{ζ}) distance; **K**) R175^{L}(H_{η})-G397^{M}(O (C=O)) distance; **L**) R175^{L}(H_{η})-L396^{M}(O (C=O)) distance. **M**) Overview of the region around the mutated site in TMH4, and the adjacent TMH5 and TMH8 (*left*: top view, *right*: front view), showing key residues in WT (red), F123L (blue), and the variant reverted back to WT (F123-to-WT, orange) in snapshots from the MD simulations. **N**) Closeup of the region around F123^{L}, showing key residues in the vicinity from MD simulation snapshots (WT in red, F123L in blue, and F123-to-WT in orange).

Table S1. Statistics on ΔpH and ΔΨ measurements. Proteoliposomes were prepared from each of three independent preparations of complex I and the F123L^{L} variant. Each liposome preparation was measured three times. The amount of incorporated enzyme varies between the individual liposome preparations and the indicated activities refer to the portion of the protein with the active side facing outward. The quenching of ACMA fluorescence is given in Δrfu min^{-1} ug^{-1} the decrease in the absorbance of the oxonol absorbance is given in ΔmAbs min^{-1} μg^{-1}. Errors are given as standard error from the mean value (s.e.m.).

Preparation	Change in ACMA fluorescence		Decrease of oxonol absorbance	
	Δrfu min^{-1} ug^{-1}	[%]	ΔmAbs min^{-1} μg^{-1}	[%]
Wild type	4.96 ± 1.16	100 ± 23	11.33 ± 2.1	100 ± 18
F123L^{L}	1.04 ± 0.31	21 ± 30	2.2 ± 0.5	20 ± 24

Table S2. Oligonucleotides used for site-directed mutagenesis. Newly generated codons are shown in bold, exchanged bases in italics. To proof the newly generated codons, silent mutations were inserted. The restriction sites are underlined. The 'check' oligonucleotide was used for DNA sequencing.

Oligonucleotides	Sequence 5'-3'	Restriction site
nuoL_F123L_fwd	CGCTTACACCAACCTG***CTC***ATCGC*T*AGCATGGTGGTTCTGGTGC	*NheI*
nuoL_F123L_rev	GCACCAGAACCACCATGCTAGCGATGAGCAGGTTGGTGTAAGCG	
check_nuoF_F123L	CCTGTCGCTGACCATG	

Table S3. List of molecular dynamics simulations.

System	Simulation	Length (ns)
WT	S1	1000
WT	S2	1000
F123L	S3	1000
F123L	S4	1000
US/WT	S5	16 windows x 20 ns (320)
US/F123L	S6	16 windows x 20 ns (320)
F123L-to-WT	S7	400
F123L-to-WT	S8	400
	Total	**5.4 µs**

Table S4. List of non-standard protonation states. The table lists protonated Asp and Glu, deprotonated Lys, and the tautomeric state of His: δ = N_δ-protonated; ε = N_ε-protonated; δ/ε = both N_δ/N_ε-protonated.

Subunit	Residue
NuoA	His12(δ), His13(δ), Asp79, Glu81, Glu102
NuoB	His76(δ)
NuoCD	His20(δ), His78(ε), His87(δ/ε), His101(ε), His123(δ/ε), Glu138, His152(ε), His167(δ), His224(ε), His228(δ/ε), His252(δ), His253(δ), His266(δ), Asp273, His319(ε), His359(δ), His370(δ), His497(δ), His511(ε), His518(ε), Glu538, His568(ε), Asp597, Asp599
NuoE	His2(δ), His24(δ), Glu25, His27(δ), His28(δ), His56(ε), His87(δ/ε), His98(δ), His150(δ), His152(δ)
NuoF	His11(δ), Asp92, Glu93, His110(ε), His172(δ), Asp298, His304(δ), His331(ε), Glu343, His400(δ), His431(ε)
NuoG	Glu23, His38(δ), His101(δ), His103(δ), Glu110, His115(ε), Asp118, His125(δ/ε), His137(δ), His148(δ), His178(ε), His213(δ), Glu243, Glu252, His261(ε), Asp266, His345(δ), Glu382, Asp383, His429(δ), His465(δ), Glu570, His574(δ), His576(δ/ε), His597(δ), His607(δ), His655(δ), His658(δ), His673(δ), Glu707, His709(δ), His724(δ), His749(δ), His819(ε), His901(δ)
NuoH	His185(δ), His208(δ), His210(ε), Glu216, Glu218, His226(ε)
NuoI	His23(δ), Glu124
NuoJ	His22(δ), His27(δ/ε), Glu55, Glu142, His157(ε), His183(δ)
NuoK	His84(ε)
NuoL	His100(δ), His207(δ/ε), His254(δ), His270(δ), His281(δ), His334(δ), His338(δ), His357(δ), His358(δ), Lys399, His411(δ), His438(δ), His444(δ), His446(δ), His453(δ), His487(δ), Glu587
NuoM	His80(δ), Glu108, His117(δ), Asp135, His159(δ), His196(δ), His241(δ/ε), His248(δ), His322(ε), His348(ε), His367(δ), His441(δ), His490(δ)
NuoN	His34(ε), His124(δ), His224(δ), His305(ε), His368(δ), Lys395, His406(δ), His435(δ)

Supplementary References

23. F. Nuber, J. Schimpf, J.P. di Rago, D. Tribouillard-Tanvier, V. Procaccio, M.L. Martin-Negrier, *et al.* Biochemical consequences of two clinically relevant ND-gene mutations in *Escherichia coli* respiratory complex I. *Sci. Rep*., 2021, **11**, 12641.
56. E. Nakamaru-Ogiso, M. C. Kao, H. Chen, S. C. Sinha, T. Yagi and T. Ohnishi, The membrane subunit NuoL(ND5) is involved in the indirect proton pumping mechanism of *Escherichia coli* complex I, *J. Biol. Chem.*, 2010, **285**, 39070-39078.
57. J. Michel, J. DeLeon-Rangel, S. Zhu, K. Van Ree and S. Vik, Mutagenesis of the L, M, and N subunits of Complex I from *Escherichia coli* indicates a common role in function, *PLoS One*, 2011, **6**, e17420.
58. M. Sato, P. K. Sinha, J. Torres-Bacete, A. Matsuno-Yagi and T. Yagi, Energy transducing roles of antiporter-like subunits in *Escherichia coli* NDH-1 with main focus on subunit NuoN (ND2), *J. Biol. Chem.*, 2013, **288**, 24705-24716.
60. R. G. Efremov and L. A. Sazanov, Structure of the membrane domain of respiratory complex I, Nature, 2011, 476, 414-420.
85. S. Bungert, B. Krafft, R. Schlesinger and T. Friedrich, One-step purification of the NADH dehydrogenase fragment of the *Escherichia coli* complex I by means of Strep-tag affinity chromatography. *FEBS Lett.*, 1999, **460**, 207-211.